Solid Earth, 11, 1969–1985, 2020
https://doi.org/10.5194/se-11-1969-2020

Solid Earth Open Access EGU

Spatiotemporal history of fault–fluid interaction in the Hurricane fault, western USA

Jace M. Koger and Dennis L. Newell

Department of Geosciences, Utah State University, Logan, UT 84322, USA

Correspondence: Dennis Lowell Newell (dennis.newell@usu.edu)

Received: 28 April 2020 – Discussion started: 25 May 2020
Revised: 23 September 2020 – Accepted: 1 October 2020 – Published: 5 November 2020

Abstract. The Hurricane fault is a ∼ 250 km long, west-dipping, segmented normal fault zone located along the transition between the Colorado Plateau and the Basin and Range tectonic provinces in the western USA. Extensive evidence of fault–fluid interaction includes calcite mineralization and veining. Calcite vein carbon ($\delta^{13}C_{VPDB}$) and oxygen ($\delta^{18}O_{VPDB}$) stable isotope ratios range from −4.5 ‰ to 3.8 ‰ and from −22.1 ‰ to −1.1 ‰, respectively. Fluid inclusion microthermometry constrains paleofluid temperatures and salinities from 45 to 160 °C and from 1.4 wt % to 11.0 wt % as NaCl, respectively. These data suggest mixing between two primary fluid sources, including infiltrating meteoric water (70 ± 10 °C, ∼ 1.5 wt % NaCl, $\delta^{18}O_{VSMOW}$ ∼ −10 ‰) and sedimentary brine (100 ± 25 °C, ∼ 11 wt % NaCl, $\delta^{18}O_{VSMOW}$ ∼ 5 ‰). Interpreted carbon sources include crustal- or magmatic-derived CO_2, carbonate bedrock, and hydrocarbons. Uranium–thorium (U–Th) dates from five calcite vein samples indicate punctuated fluid flow and fracture healing at 539 ± 10.8 (1σ), 287.9 ± 5.8, 86.2 ± 1.7, and 86.0 ± 0.2 ka in the upper 500 m of the crust. Collectively, data predominantly from the footwall damage zone imply that the Hurricane fault imparts a strong influence on the regional flow of crustal fluids and that the formation of veins in the shallow parts of the fault damage zone has important implications for the evolution of fault strength and permeability.

1 Introduction

Secondary mineralization, alteration products, and associated textures in fault rocks provide windows into past fault–fluid interaction in the crust. Fracture networks and associated sealing cements are widely recognized not only for their tectonic significance but also for their impact on fluid movement and distribution in the crust of groundwater, hydrocarbons, and ore deposits (Mozley and Goodwin, 1995; Benedicto et al., 2008; Caine and Minor, 2009; Eichhubl et al., 2009; Caine et al., 2010; Cao et al., 2010; Laubach et al., 2019). The rates, spatiotemporal evolution, and mineralogy of fracture-sealing cements in fault zones control fault zone strength, the buildup of pore pressures, the location and frequency of failure events, and the overall fault system architecture through time (e.g., Caine et al., 1996; Evans et al., 1997; Sibson, 2000). In order to constrain fault–fluid interaction during and after fault slip, we need to understand the sources of fluids moving through the systems, their temperature and chemistry, and the age of fracture in-filling minerals that aid in their healing. As highlighted in the next section, the microscopy, geochronology, stable and radiogenic isotope geochemistry, bulk rock and microscale geochemistry, and fluid inclusion analysis of diagenetic products in fault zones collectively inform these processes.

Exhumed brittle faults and fault damage zones are excellent natural laboratories for interpreting the interaction between fluids and faults with implications for fault zone permeability evolution, diagenesis, and the seismic cycle (e.g., Chester et al., 1993; Caine et al., 1996; Sibson, 1996; Caine et al., 2010; Mozafari et al., 2015; Salomon et al., 2020). Our research presented here is inspired by prior studies on exhumed normal faults in the western USA, some of which are briefly highlighted below. Although we note that many excellent examples exist worldwide in settings such as the Apennines (e.g., Ghisetti et al., 2001; Smeraglia et al., 2018), Greenland (Salomon et al., 2020), and the Dead Sea (Nuriel et al., 2012). A common theme amongst these studies is the

analyses of secondary carbonate cements and fracture-filling veins. Carbonate mineralization is amenable to radiogenic and stable isotopic analyses, whole-rock elemental analysis, fluid inclusion work, and dating, which allows for the interpretation of past fluid temperature, chemistry, sources, and timing of fluid flow in faults. For example, the Moab fault located in the northeastern Colorado Plateau is a world-class natural analog for the interplay between hydrocarbon-bearing fluid movement, and permeability evolution along a fault zone (Foxford et al., 1998). This east-dipping normal fault exhibits a protracted history of fault–fluid interaction including hydrocarbon residues and carbonate, oxide, and siliceous diagenetic cements and veins associated with deformation features. A suite of prior studies interprets multiple episodes of fluid migration and fault–rock diagenesis between the Permian and late Tertiary due to fluid expulsion from the Ancestral Rocky Mountain Paradox Basin, during Laramide deformation, and during post-Laramide extension and exhumation (Chan et al., 2000, 2001; Eichhubl et al., 2009; Bergman et al., 2013; Hodson et al., 2016).

Also located in the Colorado Plateau, the Little Grand Wash and Salt Wash faults are well-exposed examples of carbonate-cemented normal fault zones that are associated with modern-day spring emanations and are instructive as natural analogs for geological carbon sequestration (Shipton et al., 2004). Here, extensive carbonate veins, travertine spring mounds, and CO_2-rich springs and a CO_2 geyser (Crystal Geyser) are associated with normal faulting that taps a CO_2-rich fluid reservoir at depth. Fault slip, fracturing, and subsequent sealing via carbonate mineralization are interpreted to be linked to fluid pressure buildup and release. The cycle of fault slip and sealing is related to the rate of fracture filling (Frery et al., 2015) and may also be linked to changes in hydraulic head related to glacial–interglacial climatic fluctuations (Kampman et al., 2012).

To the east of the Colorado Plateau, along the Rio Grande rift, exhumed basin-bounding and intra-basin normal faults preserve a record of syntectonic changes to fault zone permeability due to groundwater flow and mineralization in poorly lithified siliciclastic sediments (Mozley and Goodwin, 1995; Heynekamp et al., 1999; Caine and Minor, 2009; Williams et al., 2015). These studies document progressive fluid flow localized along faults due to deformation and carbonate cementation that result in the compartmentalization of basin-hosted aquifers. Recent work on the Loma Blanca fault, in the south-central Rio Grande rift, documents periodic fault slip and calcite sealing using microscopy, isotope geochemistry, and uranium–thorium (U–Th) geochronology (Williams et al., 2017a, b, 2019). These studies suggest that deeply circulated, CO_2-rich fluids are focused up along this fault and that the temporal record of calcite vein fills is linked to the earthquake cycle and fault–valve behavior in this part of the Rio Grande rift.

In this contribution, we present new results documenting the paleofluid–fault interaction along the Hurricane fault zone, located at the transition between the Colorado Plateau and the Basin and Range tectonic provinces of the western USA (Fig. 1). The Hurricane fault juxtaposes Mesozoic and Paleozoic carbonates, sandstones, and shales along its strike, with excellent exposures of the footwall. Also proximal to and offset by the Hurricane fault are Pliocene–Pleistocene volcanic centers and basalt flows that may have periodically influenced the fluid flow and thermal regime near the fault (Fig. 2). Prior research on the Hurricane fault has focused primarily on its structural and paleoseismic history (Stewart and Taylor, 1996; Fenton et al., 2001; Lund et al., 2007), with studies on fault–fluid interaction limited to modern thermal springs (Crossey et al., 2009; Nelson et al., 2009). We present the first quantitative results on the spatiotemporal thermochemical evolution of paleofluid flow and fluid–rock interaction along the Hurricane fault zone using stable isotope geochemistry, fluid inclusion microthermometry, and U–Th geochronology of calcite vein networks exposed in the footwall damage zone. Our data enable us to constrain the sources and the approximately 540 ka evolution of fluid flow and fault–fluid interactions within the footwall of the Hurricane fault zone, and this study highlights the value of integrating relatively high-resolution U–Th dates with other geochemical data from fault-hosted calcite veins.

2 Geological setting of the Hurricane fault zone

The Hurricane fault zone strikes roughly north–south in the transition zone between the Colorado Plateau and the Basin and Range tectonic provinces in southwest Utah and northwest Arizona (Fig. 1). Major tectonic events that have shaped the region include the Sevier orogeny, the Laramide orogeny, and subsequent Basin and Range extension. The Sevier orogeny and the associated fold and thrust belt initiated at $\sim$ 125 Ma due to subduction and formation of a continental arc along the western margin of North America (Armstrong, 1968; Heller et al., 1986). The fold and thrust belt progressed eastward until shallowing of the subducting Farallon slab marked the onset of the Laramide orogeny at ca. 75 Ma (Livaccari, 1991; Yonkee and Weil, 2015). Laramide deformation is marked by basement-cored uplifts and the formation of the Rocky Mountains. Hydration of the continental lithosphere during this time led to widespread magmatism following foundering of the Farallon slab (Humphreys et al., 2003). Basin and Range extension and wide-spread normal faulting in the western USA began in the late Eocene (Axen et al., 1993).

Normal faults of the Basin and Range broadly follow Proterozoic accretionary and Sevier–Laramide compressional structural fabrics to accommodate late Paleogene extension (Armstrong, 1968; Quigley et al., 2002). Extension along the eastern margin of the Basin and Range adjacent to the Colorado Plateau initiated $\sim$ 15 Ma (Axen et al., 1993). The Colorado Plateau province has remained largely un-deformed by

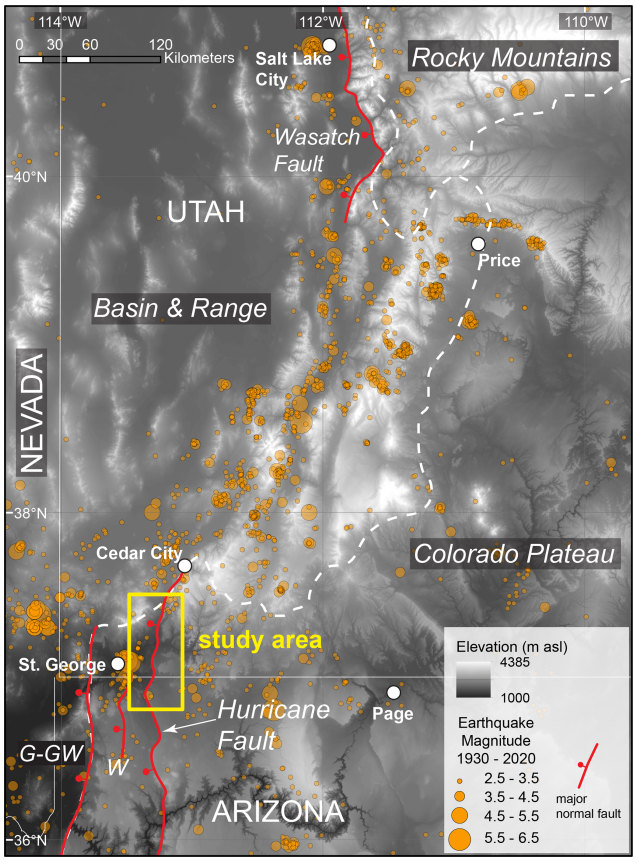

Figure 1. Location of the Hurricane fault and study area along the boundary between the Colorado Plateau and the Basin and Range tectonic provinces in the western USA. The fault is located within the Intermountain Seismic Belt as delineated by the depicted > M 2.5 earthquakes recorded between 1930 and 2020 (USGS, 2020). Other notable faults in the region include the Gunlock–Grand Wash (G–GW) and Wasatch faults. (Digital elevation, SRTM 1 Arc-Second Global https://doi.org/10.5066/F7PR7TFT, courtesy of the U.S. Geological Survey.)

Basin and Range extension, and the transition from the thick, strong crust of the Colorado Plateau to the relatively thin crust of the Basin and Range occurs over a ∼ 100 km wide interval (Zandt et al., 1995). The eastern margin of the transition zone is also coincident with the Intermountain Seismic Belt, (Fig. 1), with multiple seismically active normal faults including the Wasatch and Hurricane fault zones (Smith et al., 1989). Late Cenozoic volcanism along the margin between the two tectonic provinces is compositionally bimodal, which is indicative of high heat flow and partial melting of the mantle (Best and Brimhall, 1974).

The Hurricane fault is a 250 km long, segmented, west-dipping normal fault in southwestern Utah and northwestern Arizona with poorly constrained origins in the mid-Miocene to Pliocene (Lund et al., 2007; Biek et al., 2010). Fault activity occurred predominantly in the Pleistocene, including up to 550 m of its total 600–850 m of throw (Lund et al., 2007). Six segments of the Hurricane fault are 30–40 km long and have been defined based on geometric and structural complexities at segmentation boundaries (Fig. S1 in the Supplement to this paper; Pearthree et al., 1983; Stewart and Taylor, 1996; Stenner and Pearthree, 1999). The Hurricane fault has recently been active as evidenced by Quaternary scarps and the magnitude ∼ 5.8 earthquake that occurred in 1992 east of St. George, Utah, with a focus at a depth of ∼ 15 km along the projected dip of the Hurricane fault surface (Stewart and Taylor, 1996). Long-term slip rates based on paleoseismic studies range from 0.44 to 0.57 mm yr^{-1} (Lund et al., 2007).

Rock types juxtaposed by the fault include Paleozoic and Mesozoic sandstones, siltstones and mudstones, marine limestones, and evaporites (Biek, 2003; Biek et al., 2010). Exposures of hanging wall bedrock are broadly covered by Quaternary colluvium concealing Triassic units that are exposed in a few locations. Permian and Triassic units are well exposed in the footwall along the Hurricane cliffs, especially in canyons cutting the escarpment (Fig. S2). Units dominated by marine carbonates include the Permian Pakoon Dolomite, the Permian Toroweap Formation, and the Permian Kaibab Formation as well as lower members of the Triassic Moenkopi Formation. Siliciclastic-dominated units in footwall exposures include the Permian Queantoweap Sandstone (stratigraphically equivalent to the Hermit Formation along the southern segments of the fault), and the Triassic Moenkopi Formation. Where exposed along the fault, the Permian Queantoweap Sandstone and Hermit Formation are composed of very-fine-grained to fine-grained quartz-rich sandstone, locally cemented by calcite and/or silica and hematite.

Basaltic volcanism in the eastern Basin and Range in the transition zone to the Colorado Plateau began at ∼ 15 Ma and has been most active within the last 2.5 Myr (Nelson and Tingey, 1997). Quaternary basaltic volcanic centers are spatially associated with the Hurricane fault (Fig. 2). Basalt flows are offset by the Hurricane fault, and these are used for constraining long-term slip rates (Lund et al., 2007). Volcanic eruptions are predominantly alkali-rich basalts with lesser basaltic andesite. Neodymium isotope ratios of Quaternary basalts reflect primarily lithosphere sources along the northern half of the Hurricane fault and asthenosphere and/or mixed source to the south (Crow et al., 2011). These periods of basaltic magmatism associated with Basin and Range extension may have created hydrothermal systems in the past that locally influenced groundwater chemistry and circulation in the Hurricane fault.

Prior work on fluid movement associated with this fault is limited to geochemical and isotopic studies of modern spring systems at Pah Tempe hot springs, near La Verkin, Utah, and the Travertine Grotto and Pumpkin warm springs in the Grand Canyon. At Pah Tempe hot springs, deeply circulated meteoric waters emerge as CO_2-charged and saline fluids along the fault trace, and the precipitation of calcite veins is evident in the exhumed fault rocks (Nelson et al.,

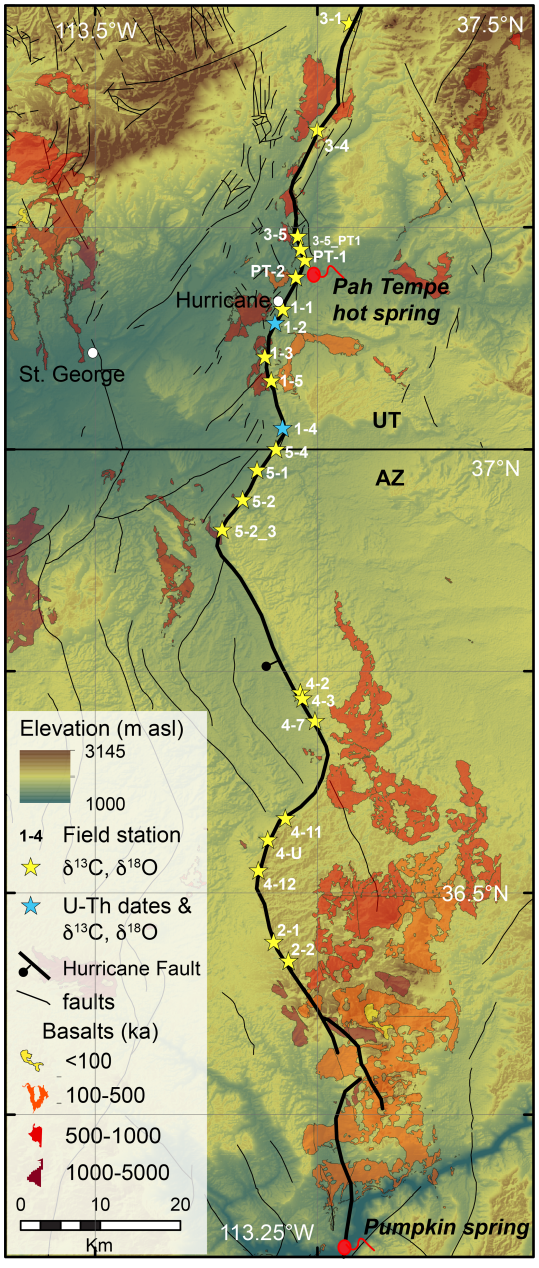

Figure 2. The Hurricane fault extent in southern Utah and northern Arizona, showing the 23 field stations investigated in this study. Note that C and O isotope values from calcite veins are reported for all field sites. Additionally, U–Th dates are reported from stations 1–2 and 1–4. The locations of Pah Tempe and Pumpkin springs are shown. Travertine Grotto is located south of the map extent. Geology was sourced from Billingsley and Workman (2000), Billingsley and Wellmeyer (2003), and Rowley et al. (2008). (Digital elevation, SRTM 1 Arc-Second Global https://doi.org/10.5066/F7PR7TFT, USGS EROS Archive, 2019, courtesy of the U.S. Geological Survey.)

2009). Travertine Grotto and Pumpkin warm springs are attributed to meteoric water mixing with deeply sourced fluids that are flowing upwards along the basement-rooted Hurricane fault (Crossey et al., 2006, 2009). Analyses of volatiles exsolving from these springs identifies a predominantly deep (endogenic) source, with some modern contributions from mantle or magmatic sources.

3 Methods

3.1 Field locations

Field investigations along the Hurricane fault were conducted between Cedar City, Utah, and the fault's intersection with the Grand Canyon in Arizona (Fig. 2). Studies were restricted to well-exposed areas of the fault's footwall, typically where canyons and drainages cross the fault. Due to colluvial cover on the hanging wall, this study focused on footwall exposures of the fault and the footwall damage zone. A total of 23 field stations (Fig. 2) along Hurricane fault were investigated, and hand samples were chosen for subsequent microscopic and geochemical characterization of diagenetic alteration and secondary vein mineralization. Sampling criteria included vein morphology; crosscutting vein relationships; varying vein and fracture orientations; and the range of apparent diagenetic modification, including unaltered host rocks. The goal was to collect a representative suite of hand samples at each of the 23 field stations to capture the range of fault–fluid interaction observable over ~ 160 km of fault length. Sample locations were recorded using a Garmin™ GPS unit in decimal degrees relative to the WGS 1984 datum (Table S1 in the Supplement). Fracture intensity (fractures per meter) in the footwall exposures were measured at each field station using linear scan line methods (e.g., Watkins et al., 2015). Fracture distance from the fault and orientation was recorded for fractures intersecting a measuring tape oriented roughly orthogonal to the fault trace. Scan line lengths were variable due to available field exposures and ranged from < 10 to ~ 400 m.

3.2 Microscopy

Standard petrographic thin sections were made from 34 hand samples displaying a range of vein types and diagenetic alteration. Of these 34 samples, 15 doubly polished thick sections (150 µm thick) of calcite veins were prepared for fluid inclusion analyses. Thin section petrographic observations were made using Leica Z16 APO and Leica DM 2700 P petrographic microscopes. Photomicrograph images were acquired with a Leica MC 170 HD camera and processed using the Leica Application Suite 4.6 software.

3.3 Fluid inclusion microthermometry

Fluid inclusions in secondary calcite mineralization were investigated using a Zeiss Universal transmitted light microscope with a Zeiss Epiplan 50x long working distance objective. A USGS gas-flow heating and freezing stage was used to measure fluid inclusion homogenization and melting temperatures. The stage was calibrated to the critical point of water using a synthetic supercritical H_2O inclusion (374.1 °C), the freezing point of a synthetic 25 mol % CO_2–H_2O inclusion (−56.6 °C), and the freezing point of double-deionized water with an ice bath (0 °C). Using the 15 thick sections, 107 homogenization temperatures (T_h) and 35 melting temperatures (T_m) were determined from two-phase fluid inclusions in calcite (Table 1).

Fluid inclusions were classified, and homogenization and melting temperatures were determined using the criteria and procedures described by Goldstein and Reynolds (1994) and Goldstein (2001). After performing heating measurements, numerous two-phase fluid inclusions with homogenization temperatures from 45 to 85 °C became metastable single-phase liquid inclusions (i.e., the bubble did not re-nucleate upon cooling). In order to re-nucleate the second phase to facilitate measurement of the melting temperatures, the fluid inclusions in these samples were intentionally stretched by heating to 110 °C for 18 h in a laboratory oven (Goldstein and Reynolds, 1994). Stretching does not impact the melting temperature because it does not alter the inclusion composition. However, if the inclusion is damaged during stretching, resulting in some water leakage, this could render melting temperatures meaningless. For a few of these treated inclusions, unreliable melting temperatures > 0 °C were obtained, and these were omitted from the data set. It is possible that stretching induced leakage from these inclusions, although this was not observed during petrographic observations. No pressure correction was performed to convert T_h measurements to trapping temperatures (T_t). Assuming vein formation at a maximum depth of 800 m equivalent to the maximum throw on the fault (Anderson and Mehnert, 1976), a maximum pressure using a lithostatic load (2675 kg m^{-3} rock density), and the maximum measured T_h of 160 °C, the pressure correction is < 10 °C (Fisher, 1976; Bakker, 2003) and is considered insignificant for this study. T_h measurements in this study are considered to be representative of the trapping temperature (T_t).

3.4 Carbon and oxygen stable isotope analysis

A Dremel® tool was used to collect 290 powdered subsamples from calcite veins, mineralized fracture surfaces, limestone host rock, and calcite-cemented sandstone host rock. Carbon and oxygen stable isotope analyses of these samples was performed in the Utah State University Department of Geosciences Stable Isotope Laboratory using a Thermo Scientific Delta V Advantage isotope ratio mass spectrometer (IRMS) and a GasBench II using the carbonate-phosphoric acid digestion method (McCrea, 1950; Kim et al., 2015). Specifically, ∼ 120–150 µg aliquots of relatively pure calcite samples and standards were placed into 12 mL Exetainer© vials and flushed with ultra-high-purity helium. Impure carbonate cements (e.g., calcite-cemented sandstone) required 300–8000 µg of sample to achieve acceptable peak amplitudes during analysis. After helium flushing, ∼ 100 µL of anhydrous phosphoric acid was added to each sample and allowed to react for 2 h at 50 °C before analysis. Carbon and oxygen stable isotope ratios were calibrated and normalized to Vienna Pee Dee Belemnite (VPDB) using the NBS-19 and LSVEC and the NBS-19 and NBS-18 international standards, respectively (Kim et al., 2015). In-house calcite standards were used to correct for drift and mass effects. Carbon and oxygen isotope ratios are reported using delta notation ($\delta^{13}C_{VPDB}$, $\delta^{18}O_{VPDB}$ values) in per mill (‰). Based on repeat analyses of in-house calcite standards, errors on $\delta^{13}C$ and $\delta^{18}O$ values are < 0.1 ‰. For calculations of paleo-groundwater $\delta^{18}O$, which are reported relative to Vienna Standard Mean Ocean Water (VSMOW), calcite $\delta^{18}O_{VPDB}$ values are converted to the VSMOW scale using Eq. (1) (Sharp, 2007):

$$\delta^{18}O_{VSMOW} = 1.03091 \cdot \delta^{18}O_{VPDB} + 30.91 \quad (1)$$

3.5 Uranium–thorium (U–Th) dating

Pilot U–Th geochronology was conducted on five key calcite vein samples from two field locations (Table S2). These include locations 1–2 and 1–4, where veins are hosted in limestone and sandstone strata, respectively (Fig. 2). Veins were slabbed with a rock saw, and approximately 300 mg of calcite powder was collected from discrete veins or vein laminations using a Dremel® tool and submitted to the University of Utah ICP-MS laboratory for analyses. At location 1–2, one laminated vein was subsampled at two locations (one near the vein wall and one near the outer part of the vein) to capture the timing of vein growth. At location 1–4, three generations of veins, determined based on crosscutting relationships, were subsampled.

Chemical preparation and analyses were performed at the University of Utah following methods modified from Edwards et al. (1987) using a Thermo NEPTUNE Plus multicollector inductively coupled plasma mass spectrometer (MC-ICP-MS). Powdered carbonate samples were dissolved in 16 M HNO_3 and equilibrated with a mixed ^{229}Th–^{233}U–^{236}U spike before being refluxed on heat for at least 1 h to ensure total dissolution. Uranium and thorium sample fractions were separated for analyses by anion exchange column chemistry. Measured peak heights were corrected for abundance sensitivities and mass bias, dark noise, background (blank) intensities, hydride contributions, ion counter yields, and spike contamination. The spike was calibrated against solutions of CRM 145 and HU1 uraninite. Uncorrected age uncertainties are reported as 1 standard error and include

Table 1. Calculated paleofluid $\delta^{13}C$ and $\delta^{18}O$ from calcite C and O stable isotopes and microthermometry.

Field station	Sample ID	$\delta^{13}C_{cc}$ ‰ (VPDB)	$\delta^{18}O_{cc}$ ‰ (VSMOW)	T_h (°C)	T_m (°C)	wt % NaCl[a]	$\delta^{13}C_{CO_2}$[b] ‰ (VPDB)	$\delta^{18}O_{H_2O}$[c] ‰ (VSMOW)
1-2	JK15HR41	0.55	22.6	102.5 ± 25.0	-7.5 ± 1.7	11.0 ± 1.4	-4.3 ± 1.1	5.6 ± 2.7
1-4	JK15HR110	0.50	10.0	75.8 ± 2.3	-2.2 ± 0.9	3.7 ± 0.5	-5.7 ± 0.1	-10.0 ± 0.3
3-1	JK15HR151	1.27	9.8	66.7 ± 11.0	-0.8 ± 0.3	1.4 ± 0.6	-5.4 ± 0.7	-11.4 ± 1.5
3-4	JK15HR160	0.35	20.2	71.6 ± 9.8	-3.2 ± 1.2	5.2 ± 1.8	-6.1 ± 0.6	-0.5 ± 1.3
3-5	JK15HR169	0.77	18.3	72.2 ± 8.7	-2.0 ± 1.9	4.7 ± 2.6	-5.6 ± 0.5	-2.3 ± 1.2
5-2	JK15HR255	1.73	13.5	70.1 ± 7.0	-1.0 ± 0.2	1.7 ± 0.7	-4.8 ± 0.4	-7.2 ± 1.0
–	Pah Tempe HS[d]	–	–	–	–	0.8	−5.5	−13.0
–	Pumpkin Spr[e]	–	–	–	–	1.1	−6.1	−10.6
	Travertine Grotto[e]	–	–	–	–	0.2	–	−10.8

[a, b, c] Calculated using Eqs. (2), (4), and (3), respectively. [d] Nelson et al. (2009). [e] Crossey et al. (2009).

measurement error and uncertainties of activity. Details of the spike calibration and data treatment can be found in Quirk et al. (2020).

4 Results

4.1 Fault zone diagenesis and veins

Evidence for fault–fluid interaction along the Hurricane fault zone exists at the macroscopic and microscopic scale. Collectively referred to as "fault zone diagenesis" (Knipe, 1992) and "structural diagenesis" (Laubach et al., 2010), these observations form the foundation of subsequent geochemical and geochronological work. Examination of the fault zone exposures at the 23 field sites (Fig. 2) reveals that it is composed of an up to 400 m wide damage zone. The damage zone (e.g., Caine et al., 1996) was qualitatively defined as the part of the exposed footwall away (east) from the main fault trace that exhibits minor slip surfaces, deformation bands, and is more intensely fractured than the unaltered host rock. We acknowledge that our assessment of the damage zone thickness is limited to the observed and available fault exposures. Exposures of the fault core (e.g., Caine et al., 1996) are less common and range from 0.5 to 2 m thick, characterized by fault breccia and gouge zones, often bounded by large slip surfaces. The record of paleofluid flow and deformation is best preserved in competent sandstone and limestone units within the damage zone, rather than finer-grained units that are typically poorly exposed. Evidence for chemical and mechanical fluid–rock interaction includes host rock alteration, veins, and mineralized and/or cemented slip surfaces, deformation bands, and breccias (e.g., Fig. 3). Secondary minerals include calcite, with lesser hematite, manganese oxides, and gypsum. Reduction (e.g., "bleaching" of sandstones; Fig. 3a, b) and oxidation features are observed in siltstone and sandstone strata with calcite and iron oxide cements. Manganese and iron-oxide vein cements, and brecciated veins are primarily observed in sandstone strata. Sparry calcite veins are the most common feature in limestone strata, with nearly every fracture hosting some calcite mineralization. The calcite veins range from single-generation millimeter to centimeter-scale sparry fracture fills to centimeter-scale laminated and fibrous veins with clear crystal terminations. Vein walls comprise intact host rocks (limestone and sandstone) and calcite-cemented breccia. Diagenetic products are most commonly associated with zones of more intense fracturing, although veins occur throughout the damage zone.

Fracture intensity varies from ~ 2 to $20\,m^{-1}$ within the Hurricane fault's damage zone. Intensely fractured zones (or corridors) of 10–$20\,m^{-1}$ are 1–2 m wide and are pervasively mineralized and "bleached" if cutting hematite-cemented sandstone. Bleaching removes hematite quartz coatings, leaving white to tan coloration in contrast to the surrounding red sandstone. Fracture orientations typically follow two main sets: one striking $0 \pm 10°$ and one striking $300 \pm 15°$, with both dipping steeply 70 to 90° (Fig. S3). The approximately north-striking fractures are generally similar to the map-scale trend of the Hurricane fault. Please refer to the Supplement for more descriptions and photos of the observed veins, features associated with fault slip, and alteration of the host rocks (Figs. S4–S6).

4.2 Vein geochemistry

4.2.1 Carbon and oxygen stable isotope ratios

Stable isotope ratios of carbon and oxygen were determined for calcite veins and host rocks from the field sites (see data repository; Newell and Koger, 2020). The $\delta^{13}C_{VPDB}$ and $\delta^{18}O_{VPDB}$ values for the entire data set range from −4.5 ‰ to 3.8 ‰ and from −22.1 ‰ to −1.1 ‰ ($\delta^{18}O_{VSMOW} = 8.1$ ‰ to 29.8 ‰), respectively (Fig. 4a). In the host rock units, carbonate cements in siliciclastic units and bulk limestone host rock were analyzed adjacent to veins and at $\sim$ 1–2 m away for comparison. Host rocks near fractures have $\delta^{13}C_{VPDB}$ and $\delta^{18}O_{VPDB}$ values from −4.5 ‰ to 2.8 ‰ and from −17.7 ‰ to −8.6 ‰, respectively. Away from fractures, host

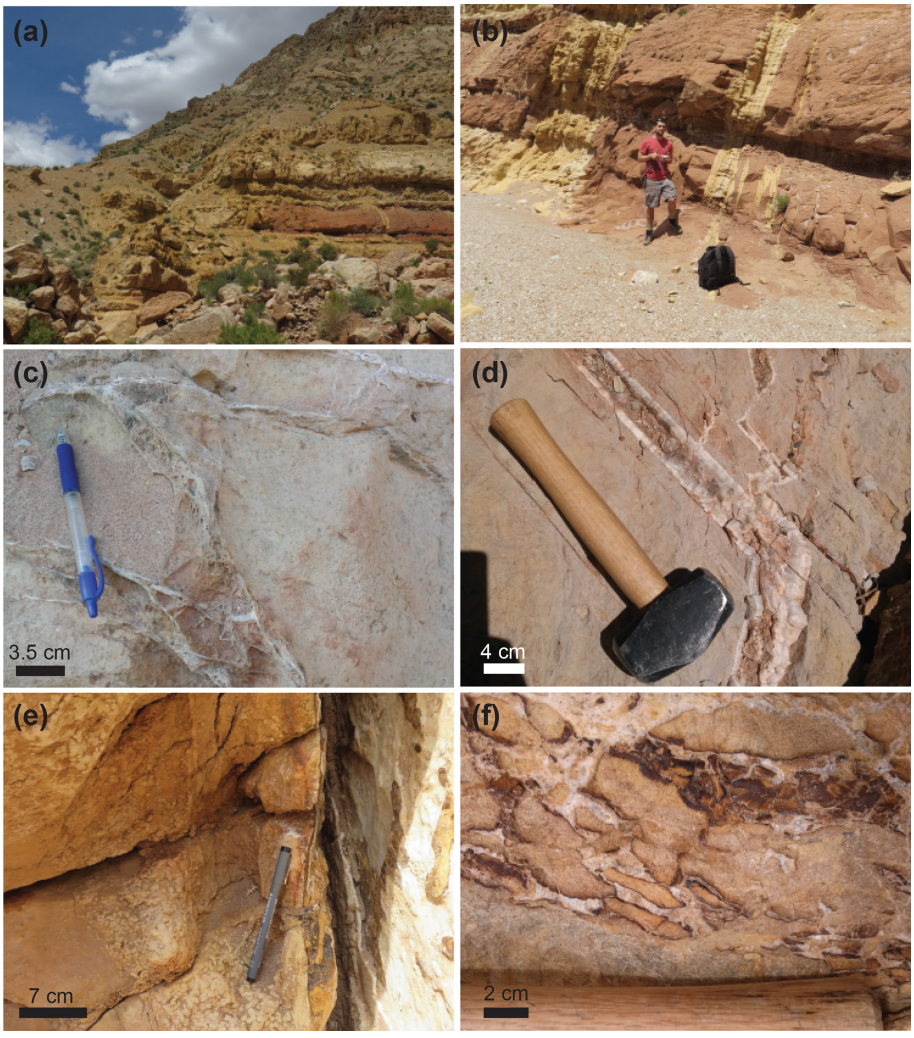

Figure 3. **(a)** Looking north along the Hurricane fault trace with colluvium in the hanging wall offset against the Permian Queantoweap Sandstone. Note the bleaching along the fault trace and in horizontal strata of the Queantoweap Sandstone. **(b)** Decimeter- to meter-scale bleached fractures cutting Queantoweap Sandstone (Jace Michael Koger used for scale). **(c)** Boxwork sparry calcite veins. **(d)** Laminated, centimeter-scale calcite vein with minor intergrown hematite cutting cherty limestone host rock. **(e)** Laminated calcite vein with minor hematite cutting Queantoweap Sandstone. Note the small calcite concretions cementing the sandstone parallel to the vein trace. **(f)** Calcite and hematite-cemented breccia in sandstone host rock.

rock $\delta^{13}C_{VPDB}$ and $\delta^{18}O_{VPDB}$ values range from -2.0 ‰ to 3.8 ‰ and from -8.5 ‰ to -1.1 ‰, respectively. The $\delta^{13}C$ and $\delta^{18}O$ values for calcite veins, breccia cements, mineralized fractures, and slip surface cements span a wide range of values with considerable scatter. For the purposes of presentation and discussion these data are divided into four "vein sets" based on common lithological associations, vein morphologic features, and $\delta^{13}C$ and $\delta^{18}O$ value data patterns (Fig. 4a; $\delta^{18}O$ values are presented versus VSMOW to facilitate comparisons to paleofluid sources). Note that these four vein sets span multiple locations (Fig. S1) and show no correlation in C and O isotope ratios with location. There is no apparent relationship between vein set and orientation (Fig. S3).

Vein set 1 calcite exhibits a positive correlation (slope = 1.6) between $\delta^{13}C_{VPDB}$ and $\delta^{18}O_{VSMOW}$ and is commonly intergrown with hematite when hosted in siliciclastic strata. Calcite in set 2 also displays a positive $\delta^{13}C_{VPDB}$ and $\delta^{18}O_{VSMOW}$ correlation (slope = 0.9) with $\delta^{13}C$ shifted to lower values compared with vein set 1. Set 3 has a wide range of isotopic values, showing no strong trends or patterns. Set 4 calcite $\delta^{18}O$ values that overlap with set 3, with $\delta^{13}C$ values that trend to significantly lower values. The majority of set 4 data are from location 1–2.

4.2.2 Fluid inclusion microthermometry

Of the 15 thick sections of calcite veins observed, six contain populations of two-phase fluid inclusions that yield ho-

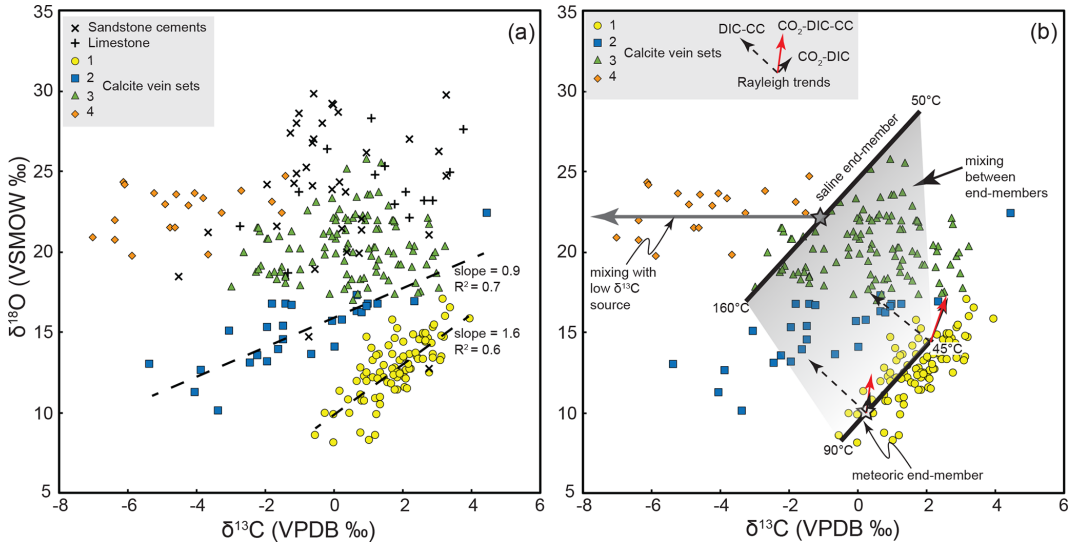

Figure 4. **(a)** Calcite $\delta^{18}O_{VSMOW}$ and $\delta^{13}C_{VPDB}$ values for veins and host rocks along the Hurricane fault. Host rock values are from bulk limestone samples and from calcite-cemented sandstones. The veins are divided into four veins sets for analysis. Note the trend line slopes for vein sets 1 and 2. **(b)** Paleofluid interpretations integrating the isotopic and fluid inclusion microthermometry results. Mixing scenarios depicted include the mixing of two end-member fluids over a range of temperature and the mixing with a low-$\delta^{13}C$ CO_2 source. Also shown are the Rayleigh fractionation trends (arrows) due progressive precipitation of calcite from water-dissolved inorganic carbon (DIC-CC), progressive CO_2 loss from the water-dissolved inorganic carbon (CO_2-DIC), and the combined effects of CO_2 degassing and calcite precipitation (CO_2-DIC-CC). The Rayleigh trends are computed for F from 1 to 0 (e.g., Eq. 4).

mogenization (T_h) and melting (T_m) temperatures (Table 1, Fig. 5). Homogenization temperatures are used to approximate the trapping temperature (T_t) and are representative of fluid temperatures during mineralization. Melting temperatures depend on the nature and concentration of dissolved species and are used to estimate the salinity of paleofluids (Bodnar, 1993).

Fluid inclusion homogenization and melting temperature data are organized by the calcite vein set as described in Sect. 4.2.1. Observed two-phase fluid inclusions range from ∼ 5 to 40 µm on the long axis. Most inclusions are interpreted to be primary and there are few trails of secondary inclusions. Single-phase (water) fluid inclusions are also present with long axis dimensions < 15 µm. Homogenization temperatures for set 1 two-phase inclusions range from 45 to 90 °C. Vein set 3 samples have two-phase fluid inclusion homogenization temperatures from 55 to 160 °C, and their distribution skews towards lower temperatures, with a mode at 65–70 °C. Only single-phase fluid inclusions are present in vein sets 2 and 4. Trapping temperatures for single-phase inclusions cannot be readily determined. Trapping temperatures are often inferred as < 50 °C (Goldstein and Reynolds, 1994; Goldstein, 2001); however, small inclusions (< 10 µm) can fail to nucleate a bubble up to ∼ 140 °C (Krüger et al., 2007). Ice melting temperatures from vein set 1 range from −3 to 0 °C, equating to a salinity of 0 wt % to 5 wt % as NaCl (Fig. 5). Calcite set 3 yields melting temperatures from −11 to 0 °C, equating to 0 wt % to 15 wt % NaCl. As no initial

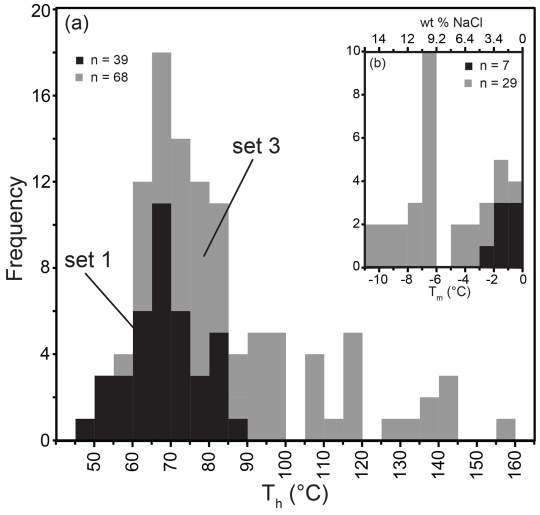

Figure 5. **(a)** Fluid inclusion (two-phase) homogenization temperatures from vein set 1 and 3. **(b)** Fluid inclusion melting temperatures from vein sets 1 and 3 and the calculated salinity (as wt % NaCl; see text for details).

melting was observed, NaCl-dominated salinity is assumed and is calculated using the equation of Bodnar (1993).

4.3 U–Th geochronology

The U–Th dates from the five vein samples range from 86 to 539 ka (Table S2). More specifically, the laminated cal-

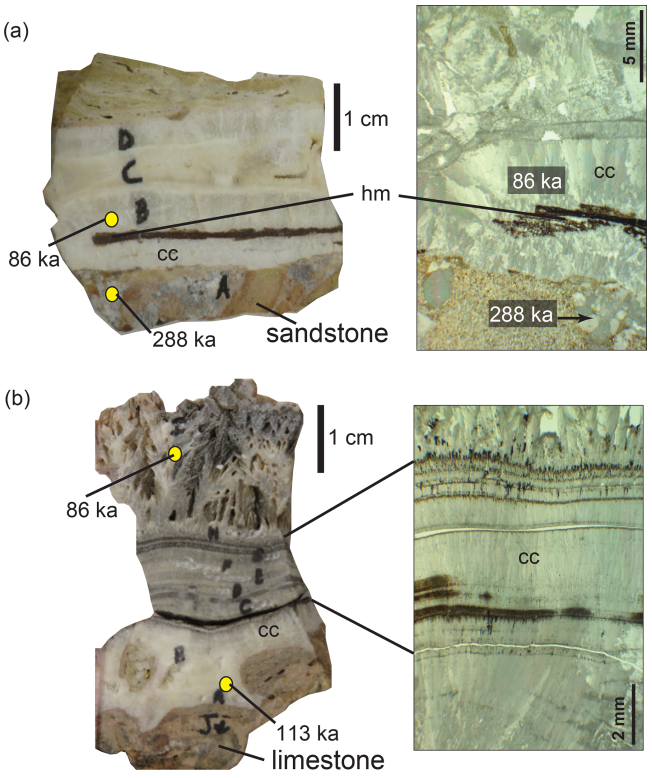

Figure 6. **(a)** Laminated calcite vein from location 1–4 and the associated U–Th dates (samples JK15HR110 and JK15HR111). The hand specimen (left) and plane-polarized photomicrograph (right) are shown. Note the calcite-cemented brecciated sandstone forming the vein wall. The laminated calcite vein shows at least four episodes of calcite precipitation. The calcite cement in the wall breccia is 288 ka and the first lamination growing on the vein wall is 86 ka. **(b)** Laminated calcite vein from location 1–2 that is hosted in marine limestone. U–Th dates (JK15HR27 and JK15HR35) are shown on the hand specimen. The dates indicate growth outward from the limestone wall from 113 to 86 ka. Multiple dense laminations are visible in the hand sample, and the plane-polarized photomicrograph shows that these are constructed of fibrous calcite crystals that terminate at discrete boundaries. The outermost (86 ka) layer is characterized by higher porosity vuggy calcite crystals suggestive of growth into free fluids.

cite vein from location 1–2, hosted in limestone strata, yields an inner lamination date of 113.1 ± 0.3 ka (1σ error) and an outer lamination date of 86.2 ± 1.7 ka (Fig. 6). The three calcite veins at location 1–4, hosted in sandstone strata, yield dates of 539 ± 10.8, 287.9 ± 5.8, and 86.0 ± 0.2 ka in chronological order consistent with crosscutting relationships. Two dates from a single sample include calcite cement from a brecciated vein wall (288 ka) that is crosscut by a laminated calcite vein (86 ka) (Fig. 6). In the field, this vein crosscuts the 539 ka vein.

5 Discussion

5.1 Paleofluid sources in the Hurricane fault

The carbon and oxygen stable isotope ratios of the calcite veins can inform the groundwater composition, source, and processes at work during paleofluid circulation in the Hurricane fault. The C and O equilibrium isotopic fractionation between CO_2 and calcite (CO_2–cc) and water and calcite (H_2O–cc), respectively, are temperature dependent, and assuming that isotopic equilibrium during mineralization is valid, additional information on the paleofluid temperature is needed to proceed. Homogenization temperatures of primary two-phase fluid inclusions in calcite, when present, are a reliable method to estimate temperature and, thus, to calculate the paleofluid O and C isotopic composition using Eqs. (2) and (3):

$$\text{O isotopes: } 1000 \ln \alpha_{H_2O\text{-cc}} = 2.89 - \frac{2.78 \times 10^6}{T^2} \quad \text{(O'Neil et al., 1969, 1975)} \tag{2}$$

$$\text{C isotopes: } 1000 \ln \alpha_{CO_2\text{-cc}} = 3.63 - \frac{1.194 \times 10^6}{T^2} \quad \text{(Deines et al., 1974).} \tag{3}$$

Here, α_{x-y} is the temperature-dependent fractionation factor between water and calcite (H_2O–cc) and between CO_2 and calcite (CO_2–cc), and T is temperature in Kelvin. For the fractionation factor magnitudes expected for these two systems, the difference in delta values between the phases (i.e., $\delta^{18}O_{H_2O} - \delta^{18}O_{cc}$ and $\delta^{13}C_{CO_2} - \delta^{13}C_{cc}$) is a good approximation for $1000 \ln \alpha$ (Sharp, 2007). For these calculations, $\delta^{18}O$ and $\delta^{13}C$ values are on the VSMOW and VPDB scales, respectively. When fluid inclusion data are not available, temperatures may be estimated based on other constraints, such as estimates of mineralization depths and the geothermal gradient, but the resulting paleofluid isotopic estimates will be far more uncertain due to surface-ward advection of geotherms (Forster and Smith, 1989). Clumped carbonate isotopic methods (Δ_{47}) can yield reliable temperature estimates from fault zone calcite mineralization (Swanson et al., 2012; Hodson et al., 2016), but they are not available for this study. In the absence of these constraints, a range of temperatures or starting fluid isotopic compositions can be explored to provide some interpretations of the calcite stable isotope data, again resulting in considerable uncertainty.

For the six samples that hosted populations of two-phase fluid inclusions, microthermometry heating and freezing data are used to estimate the fluid trapping temperatures and salinities of the paleofluids present in the Hurricane fault. In combination with $\delta^{18}O_{VSMOW}$ values from the calcite hosting these fluid inclusions, the paleofluid $\delta^{18}O_{VSMOW}$ values are calculated using Eq. (2). Although calcite oxygen stable isotope measurements are conducted on micro-drilled aliquots, these are still bulk samples when considering the micro-

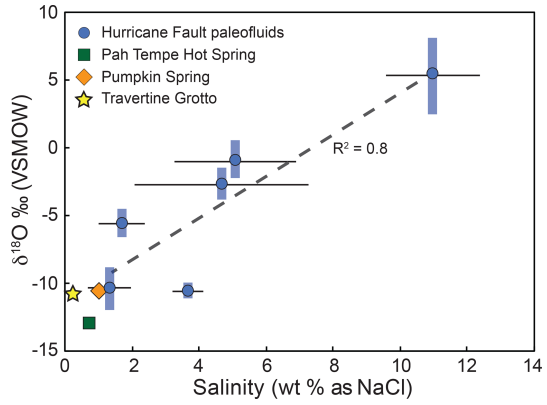

Figure 7. Calculated paleofluid oxygen isotope composition versus fluid salinity determined by fluid inclusion microthermometry. The strong positive correlation of δ^{18}O and salinity ($R^2 = 0.8$) is interpreted as a mixing trend between the low-salinity, meteoric water and the high-salinity sedimentary brine end-member. For comparison, the composition of Pah Tempe, Pumpkin, and Travertine Grotto springs are included and are very similar in composition to the low-salinity end-member.

scopic distribution of fluid inclusions. Also, in each sample, the microthermometry results yield populations of fluid inclusions with some variation in homogenization temperature. Therefore, we cannot connect individual isotopic values to individual fluid inclusions. Rather, we use the mean and standard deviation of measured temperatures in each sample along with the calcite $\delta^{18}O_{VSMOW}$ value to estimate a range of paleofluid compositions (Table 1). Similarly, we associate this range of oxygen isotope values with the mean and standard deviation of the paleofluid salinity as estimated from fluid inclusion melting temperatures. The paleofluid $\delta^{18}O_{VSMOW}$ value and salinity (wt % as NaCl) estimates for these samples show a strong positive correlation ($R^2 = 0.8$; Fig. 7). We interpret this correlation as mixing between two end-member fluid types as well as the fact that, over the history of fault–fluid interaction represented by these calcite veins, different proportions of $\sim 100 \pm 25$ °C, saline ($\sim$ 11 wt % NaCl), high-$\delta^{18}O_{VSMOW}$ (~ 5 ‰) fluids have mixed with 70 ± 10 °C lower-salinity (~ 1.5 wt % NaCl), lower-$\delta^{18}O_{VSMOW}$ (~ -10 ‰) ground waters.

We suggest that the end-member characterized by high δ^{18}O values and high salinity is consistent with sedimentary formation water (brine) that originated from extensive meteoric water–rock interaction and oxygen isotope exchange with marine sedimentary sequences (e.g., Clayton et al., 1966). Assuming a 25–30 °C geothermal gradient and the range of fluid inclusion temperatures, the circulation depths for these ground waters ranges from 2 to 6 km. This geothermal gradient is consistent with most observations from geothermal exploration wells in the region (Sommer and Budding, 1994). This is adequate to infiltrate all of the Mesozoic and Paleozoic strata in the region, including thick sections of marine carbonate and evaporite bearing units (Biek, 2003; Dutson, 2005; Biek et al., 2010). Infiltration into these marine units is a likely source of the salinity in these ground waters. The end-member characterized by relatively low salinity and a low δ^{18}O value is likely dominantly meteoric water. Using the same geothermal gradient, these ground waters have circulated to ~ 3.5 km based on fluid inclusion constraints. For comparison, Pah Tempe hot springs (Nelson et al., 2009) and Pumpkin and Travertine Grotto springs (Crossey et al., 2009) emanate along the Hurricane fault and have a similar oxygen isotope composition and salinity to this end-member (Fig. 7). Based on comparisons of Pah Tempe hot springs δ^{18}O and δ^{2}H values with other local and regional meteoric waters, Nelson et al. (2009) interpret the source of the hot spring water as meteoric water that infiltrated during the last glacial interval. Based on geochemical geothermometry estimates and the observed shift in hot spring water to higher δ^{18}O values, Nelson et al. (2009) suggest that Pah Tempe thermal waters circulate to depths of 3–5 km with temperatures of 70–150 °C. This approach has also been employed at other faults to interpret paleofluid compositions. For example, coupled fluid inclusion microthermometry and stable isotope values from fault-hosted calcite along the Moab fault, Utah, USA, point to a mixing process between upwelling basin brines with meteoric water (Eichhubl et al., 2009). Although we suggest that the saline fluids in the Hurricane fault are the product of water–rock interaction, it is important to note that an alternative interpretation is mixing between meteoric water and basin brine derived from the evaporation of paleo-seawater. The "high-salinity" end-member that we observe is consistent with basin brines, albeit on the low end of observed salinities (e.g., Bodnar et al., 2014). It is possible that we have not captured the true high-salinity end-member in our sampling. To further evaluate the source of the saline fluids, additional data that are currently not available, such as halogen content and isotopic composition (e.g., Cl/Br, δ^{37}Cl value), may be diagnostic (e.g., Yardley et al., 2000).

In terms of the carbon sources in these two fluids, there are alternative ways of interpreting the relatively narrow range of calcite $\delta^{13}C_{VPDB}$ values (0.35 ‰ to 1.73 ‰). First, using the average calcite formation temperatures from fluid inclusions, we estimate the $\delta^{13}C_{VPDB}$ of dissolved CO_2 in the paleofluid from -6.1 ‰ to -4.3 ‰ using Eq. (3) (Table 1). However, unlike the oxygen isotope system that most likely reflects the water composition, carbon composition can be reflective of a carbonate host rock. For example, dissolved carbonate in equilibrium with limestone bedrock (i.e., strongly buffered by the host rock) will result in calcite veins with a δ^{13}C similar to the host limestone (e.g., Dietrich et al., 1983). In this case, calculating the carbon isotopic composition of an external CO_2 source may not be appropriate, and the vein value is simply representative of the source carbon. In this study, the host rock limestone $\delta^{13}C_{VPDB}$ values range from -2.7 ‰ to 3.8 ‰ with an average of 1.2 ‰, which is in the range of

expected values from marine carbonates (e.g., Hoefs, 1987; Sharp, 2007). However, in parts of the fault that have higher water–rock ratios or are generally carbonate poor (e.g., siliciclastic host rock), the carbon isotopes of calcite veins can be representative of an external CO_2 source that is dissolved and traveling in the groundwater. With these uncertainties in mind, we interpret the end-member carbon sources for the calcite veins as external CO_2 sources and local marine limestones. Based on the results from this study, there may be a weak association between the two carbon sources and the fluid end-members based on oxygen isotopes and salinity. In some but not all cases, vein $\delta^{13}C$ values that are similar to host limestone tend to be associated with the highest salinity fluids. Veins hosted in sandstone units and associated with an external CO_2 source (~ -6 ‰) are associated with the lower-salinity fluids in most cases. These carbon isotope values are similar to the observed $\delta^{13}C_{VPDB}$ values of CO_2 at Pah Tempe (-5.5 ‰) and Pumpkin (-6.1 ‰) springs (Crossey et al., 2009; Nelson et al., 2009). These values overlap with mantle CO_2 values (Marty and Jambon, 1987), but they are also similar to values observed in many crustal fluids and continental hot springs globally (Sherwood Lollar et al., 1997; Ballentine et al., 2002; Newell et al., 2008, 2015). Based on helium and carbon isotopes, Crossey et al. (2009) and Nelson et al. (2009) suggest that mantle CO_2 could range from a just a few percent to as high as ~ 40 % in the Hurricane-fault-hosted hot springs, depending on the mantle and crustal end-members used. We do not have constraints on the helium isotope ratios of the paleofluids, so we cannot further evaluate the possibility of magmatic contributions.

5.2 Subsurface processes impacting isotopic values

As shown earlier, the $\delta^{13}C$ and $\delta^{18}O$ values from calcite veins and cements associated with the Hurricane fault display a large range of values (Fig. 4a). In addition to the binary mixing described in Sect. 5.1, precipitation of calcite from fluids with a range of temperatures is occurring along flow paths. A fairly wide range of temperatures is evident from the fluid inclusion work on vein sets 1 and 3. For a given water $\delta^{18}O_{VSMOW}$ and $\delta^{13}C$ (of dissolved CO_2), varying temperature in Eqs. (2) and (3) results in trends in calcite $\delta^{18}O_{VSMOW}$ and $\delta^{13}C_{VPDB}$ with a slope of ~ 2.3 (Fig. 4b). To explore the impacts of both temperature change and mixing, the calcite forming from the saline ($\delta^{18}O_{VSMOW} = 5$ ‰) and meteoric water ($\delta^{18}O_{VSMOW} = -10$ ‰) end-members, both with a $\delta^{13}C_{VPDB} = -6$ ‰, are superimposed on the observed data (Fig. 4b, shaded region). The vein set 1 pattern is fairly well matched by calcite forming over a the range of T consistent with the fluid inclusion measurements (90–45 °C) from the low-salinity meteoric water end-member ($\delta^{18}O_{VSMOW} = -10$ ‰; $\delta^{13}C_{VPDB} = -6$ ‰). The scattered values observed for vein set 3 are encompassed by the calcite forming from mixed saline and meteoric fluids over the range of temperatures consistent with the fluid inclusion measurements (160–50 °C). Although not shown in the diagram, using a limestone-buffered $\delta^{13}C_{VPDB}$ (~ 1 ‰) predicts values that are *not* consistent with any of the observed data, and this suggests that an external source of CO_2 may be most appropriate for veins in both the carbonate and siliciclastic host rock. The vein set 4 isotopic values are best explained by mixing the saline end-member at ~ 100 °C with a $\delta^{13}C_{VPDB}$ source of ~ -12 ‰ (Fig. 4b). This low $\delta^{13}C$ value is consistent with derivation from organic matter (Boles et al., 2004). Hydrocarbons are present regionally and in the strata that hosts the Hurricane fault (Bahr, 1963; Blakey, 1979). Mobilization and microbial oxidation of these hydrocarbons to form dissolved carbonate (Baedecker et al., 1993; Tuccillo et al., 1999) has been shown in other fault settings to form calcite veins with low $\delta^{13}C$ values (e.g., Eichhubl et al., 2009).

In addition to fluid mixing over a range of temperatures, other processes that occur during vein formation can also result in a range of calcite O and C stable isotope values. For example, open-system (Rayleigh) CO_2 degassing and calcite precipitation results in progressive fractionation of C and O stable isotopes in the fluid that result in correlations between $\delta^{13}C$ and $\delta^{18}O$ values (Hendy, 1971). Kampman et al. (2012) used a Rayleigh fractionation model, assuming isotopic equilibrium, to describe C and O stable isotope values observed in fault-controlled aragonite veins and travertine deposits in the Salt Wash graben, Utah, USA. In this system, coupled CO_2 degassing and carbonate precipitation from a homogenous CO_2-charged fluid source can explain the positive correlation and range in $\delta^{13}C$ and $\delta^{18}O$ values. In combination with U–Th geochronological constraints, these authors suggest that this system has been active periodically for > 100 kyr with a consistent paleofluid source and isotopic composition.

We test if the positively correlated C and O values observed for vein set 1 (slope = 1.6) and set 2 (slope = 0.9) (Fig. 4a) can be explained by similar processes. Rayleigh fractionation trends are included on Fig. 4b for calcite resulting from CO_2 degassing (CO_2-DIC), coupled CO_2 degassing and calcite precipitation (CO_2-DIC-CC), and calcite precipitation from groundwater (DIC-CC). These are calculated for both the carbon and oxygen isotope system using a Rayleigh distillation approach similar to Kampman et al. (2012). For example, for the progressive formation of calcite from bicarbonate, the carbon isotope ratios can be calculated from Eq. (4):

$$\delta^{13}C = \delta^{13}C_o - [1000 \times \ln \alpha_{\text{product-HCO}_3} (1 - F)], \quad (4)$$

where $\delta^{13}C_o$ is the starting carbon isotope ratio for HCO_3^- in solution, and F is the fraction of the C remaining in solution. Temperature-dependent equilibrium fractionation factors (α) for carbon isotopes in the calcite–CO_2–dissolved inorganic carbon (DIC) system are derived from Deines et al. (1974). We assume that the paleofluids were slightly acidic (~ 6.5) and near the equivalence point of H_2CO_3 and HCO_3^- to compute the $\alpha_{DIC\text{–}CO_2}$ (Gilfillan et al., 2009). This is consistent with pH and geochemical observations at Pah Tempe hot

springs and Pumpkin spring (Crossey et al., 2009; Nelson et al., 2009). Assuming the precipitation of calcite based on $CaCO_{3(calcite)} + CO_{2(g)} + H_2O \Leftrightarrow 2HCO^-_{3(aq)} + Ca^{2+}_{(aq)}$, the formation of calcite from HCO_3^- in solution partitions, on a molar basis, the carbon equally between calcite and CO_2. Using the approach of Kampman et al. (2012), the net fractionation factor between the products and the bicarbonate in solution based on Eq. (5) is

$$\alpha_{\text{product-HCO}_3} = 1/2(\alpha_{\text{calcite-HCO}_3^-}) + 1/2(\alpha_{\text{DIC-CO}_2}) \quad (5)$$

Similarly, the oxygen isotope fractionation factor is calculated using Eq. (6):

$$\alpha_{\text{product-HCO}_3} = 1/3(\alpha_{\text{CO}_2\text{-HCO}_3}) + 1/2(\alpha_{\text{calcite-HCO}_3}) + 1/6(\alpha_{\text{H}_2\text{O-HCO}_3}) \quad (6)$$

The oxygen isotope system temperature-dependent fractionation factors are derived from published relationships (O'Neil et al., 1969, 1975; Beck et al., 2005).

Focusing on vein set 1 and a range of temperatures observed from fluid inclusion, the computed trends alone cannot explain the observed data (Fig. 4b). Rayleigh fractionation trends under equilibrium conditions for CO_2 degassing and coupled CO_2 degassing + calcite precipitation $< 85\,^\circ$C yield positive correlations that are *not* similar to the observed slope or the wide range of values in set 1 calcite veins. Progressive calcite precipitation without CO_2 degassing produces *negative* correlations in δ^{13}C and δ^{18}O. Based on this analysis, it is unlikely that these processes are primary phenomena involved in the formation of calcite veins in the Hurricane fault zone. However, it is reasonable to assume that these processes are operable and impart a secondary control on the isotopic values observed from the fluid mixtures and may assist in explaining some of the data variability. It is important to note that these Rayleigh fractionation models assume isotopic equilibrium. Rapid degassing and calcite precipitation may result in disequilibrium and kinetic fractionation that cannot be quantitatively addressed and that could produce a wider range of isotopic values. However, rapid degassing would likely produce populations of vapor-dominated fluid inclusion along with liquid-dominated inclusions in the calcite veins, which are not observed.

To summarize these analyses and interpretations, most of the vein C and O isotopic compositions and trends observed can be explained by a combination of the mixing of two primary fluid end-members over a range of temperatures, with second-order impacts from processes such as degassing during calcite precipitation. It is important to note that all of these processes would occur under open-system conditions in the fault zone. Vein set 1 is best explained by formation over a range of temperatures from the low-salinity end-member. Most of the values in set 2 and 3 can be explained by a mixture of the low-salinity meteoric and the sedimentary brine end-members and precipitation over a range of temperatures. Vein set 4 requires addition of a much lower δ^{13}C component to the fluids responsible for vein set 3, likely derived from an organic source.

5.3 Implications of vein geochronology

Pilot U–Th geochronology on five samples indicates that calcite veins formed from 539 to 86 ka. These samples are from two different sample locations (1–2 and 1–4), separated by 13 km along strike (Figs. 2, 6), and from vein sets 1, 3, and 4. Specifically, at location 1–2, hosted in limestone, calcite vein growth occurred at 133 and 86 ka (set 4). Based on the interpreted growth direction of this vein, the dated laminations are chronologically consistent and suggest that the numerous vein laminations formed over a period of ~ 47 ka (Fig. 5b). At location 1–4, hosted in sandstone, veins formed at 539 and 288 ka (set 1) and 86 ka (set 3). As described in the results, the dates are consistent with interpreted observed crosscutting relationships, including the 86 ka calcite lamination cutting 288 ka calcite-cemented brecciated sandstone (Fig. 6a).

Based on the stable isotope results and analyses, the 539 and 288 ka veins are likely associated with the low-salinity meteoric water end-member (Fig. S7) and formed at moderate temperatures (60–70 °C). The 113 ka and both 86 ka veins are best associated with $\sim 100\,^\circ$C saline groundwater, with varying contributions of a low-δ^{13}C carbon source (Fig. S7). The 86 ka sample from location 1–2 has the lowest δ^{13}C (-7 ‰) observed in this study and, as discussed in Sect. 5.2, requires an organic carbon source not observed at other locations.

Although this data set is small, it suggests punctuated vein-forming events with some consistency along fault strike. Interestingly, these two fault locations appear to preserve the 86 ka fluid flow event, within analytical error, with both requiring similar composition and temperature fluids, suggesting that the fluid circulation events have continuity over at least ~ 13 km of fault zone strike. More geochronological work is needed to evaluate if these crosscutting relationships are more broadly consistent along the fault zone. These dates can be used along with constraints on fault slip rate to estimate the maximum depth of vein formation. Using the published slip rate estimates of 0.44 to 0.57 mm yr^{-1} (Lund et al., 2007), this equates to vein formation depths from ~ 40 to 300 m. However, this assumes negligible exhumation of the footwall over the last 540 ka, and they are minimum estimates. Using the local incision rate of the Virgin River through the footwall of 338 m Myr^{-1} (Walk et al., 2019) as a maximum estimate of footwall exhumation, this suggests a maximum depth of vein formation from 70 to 480 m. Consistent with the findings at thermal springs along the Hurricane fault zone (Crossey et al., 2006; Crossey et al., 2009; Nelson et al., 2009), this indicates that deeply circulated thermal fluids are moving up the fault zone, advecting deeper geotherms towards the surface, and mixing with shallow meteoric fluids. The relatively shallow depth of these processes is notable, and has been observed at other major normal faults. For ex-

ample, Smeraglia et al. (2018) documented Pleistocene synkinematic calcite mineralization along the Val Roveto fault (Apennines, Italy) that formed within the upper 350 m of the fault zone during mixing of deeply derived fluids and meteoric infiltration.

Although not the primary objective of this paper, the calcite vein textures in the context of the preliminary geochronological results warrant a brief discussion. The vein wall breccias and laminated calcite veins observed along the Hurricane fault share similar characteristics to those in other major fault zones that have been attributed to coseismic or post-seismic sealing (e.g., Nuriel et al., 2011, 2012; Smeraglia et al., 2018). These fracture openings filled with laminated growth bands of fibrous calcite crystal are indicative of post-fracture opening sealing (crack-seal cycle; Ramsay, 1980). These suggest fluid pressurization and fluid flow cycles associated with periodic fracturing in the fault damage zone, possibly due to seismic activity (e.g., Sibson, 1994). Williams et al. (2017b) showed that detailed U–Th dating of these types of laminated veins inform the periodic nature of fracture opening and sealing via calcite precipitation and argue that these are associated with seismic events. Specifically, they documented 13 seismic events between 550 and 150 ka and use this to estimate long-term earthquake recurrence intervals. In addition to earthquakes, Pleistocene climatic cycles could influence groundwater flow and fluid pressure and could possibly be associated with vein-forming events similar to what is observed at the Little Grand Wash and Salt Wash faults (e.g., Kampman et al., 2012). We have documented four such events in the last $\sim$ 540 ka, suggesting that a similar high-resolution geochronological study could yield meaningful information about the long-term recurrence of fluid-flow-triggering events along the Hurricane fault zone, whether triggered by seismicity or linked to climatic cycles.

6 Summary and conclusions

Integrated calcite vein stable isotope geochemistry, fluid inclusion microthermometry, and U–Th geochronology document the nature of paleofluids circulating in the Hurricane fault over the last $\sim$ 540 kyr. Our results indicate that calcite veins form in the footwall damage zone of the fault from mixtures of two main fluids over a range of temperatures and that processes such as CO_2 degassing may influence vein formation from the fluid mixtures. These include a relatively low-salinity meteoric-affinity groundwater and a salty sedimentary formation water. Carbon sources are more ambiguous, but they likely include significant contributions from crustal or magmatic CO_2 and carbonate bedrock, along with lesser amounts from hydrocarbons. Fluid inclusion microthermometry temperatures from $\sim$ 45 to 160 °C indicate that these fluids have circulated deeply (up to 6 km) prior to flowing up the Hurricane fault zone. Our pilot geochronology is sparse (five dates) but supports punctuated vein-forming events at 539, 288, 113, and 86 ka. Considering the published long-term slip rates along the Hurricane fault, these veins likely formed in the upper $\sim$ 500 m of the crust. Present-day upflow of similar composition fluids occurs at Pah Tempe hot springs and where the fault cuts the Colorado River in the Grand Canyon at the Pumpkin and Travertine Grotto springs.

These results have implications for how the paleohydrology of the Hurricane fault changes spatially and through time. Calcite-cemented fault breccia and laminated, fibrous calcite veins are suggestive of cycles of fracture opening and healing (i.e., crack-seal textures). Deep groundwater circulation and fault processes result in high pore pressures in the fault zone, and subsequent fracturing triggers the upflow of CO_2-charged thermal fluids, fluid–rock interaction in the fault zone, and mixing with other ground waters. Calcite mineralization and veining from these flowing fluids heal breccias and fractures. The multiple generations of crosscutting veins and laminated veins indicate that healed parts of the fault have experienced this cycle multiple times and that these processes have strongly impacted the flow properties of the fault zone. Data from this study show that these linked mechanical and hydrological processes are occurring in the upper $\sim$ 500 m of the fault zone and are occurring periodically over $\sim$ 180 km of fault strike. We conclude that the Hurricane fault imparts a strong influence on regional flow of crustal fluids and that the formation of veins in the shallow parts of the fault damage zone has important implications for fault strength in the uppermost part of the crust.

Data availability. Readers are invited to access the full data set archived on the EarthChem Library: https://doi.org/10.26022/IEDA/111542 (Newell and Koger, 2020).

Supplement. The supplement related to this article is available online at: https://doi.org/10.5194/se-11-1969-2020-supplement.

Author contributions. JMK conducted the field sample collection, sample preparation, and sample analyses as part of the requirement for his MSc in Geology from Utah State University (Koger, 2017). DLN was the thesis supervisor, provided assistance and mentorship on sampling and analytical techniques, contributed guidance with respect to data analysis, and is the corresponding author for the preparation of this paper.

Competing interests. The authors declare that they have no conflict of interest.

Special issue statement. This article is part of the special issue "Faults, fractures, and fluid flow in the shallow crust". It is not associated with a conference.

Acknowledgements. We thank Andrew Lonero (USU Geosciences) and Diego Fernandez (University of Utah) for their assistance with stable isotopic and U–Th analyses, respectively. Funding for this research was provided by a Geological Society of America Student Research Grant to Jace Michael Koger and the Department of Geosciences at USU. This paper greatly benefitted from constructive reviews by Billy Andrews, Matthew Steele-MacInnis, and the topical editor Peter Eichhubl.

Review statement. This paper was edited by Peter Eichhubl and reviewed by Matthew Steele-MacInnis and Billy Andrews.

References

Anderson, R. E. and Mehnert, H. H.: Reinterpretation of the history of the Hurricane fault in Utah, in: Basin and Range Symposium, edited by: Newman, G. W., Rocky Mountain Association of Geologist and Utah Geological Association, Denver, CO, 145–165, 1976.

Armstrong, R. L.: Sevier orogenic belt in Nevada and Utah, Geol. Soc. Am. Bull., 79, 429–458, 1968.

Axen, G. J., Taylor, W. J., and Bartley, J. M.: Space-time patterns and tectonic controls of Tertiary extension and magmatism in the Great Basin of the western United States, Geol. Soc. Am. Bull., 105, 56–76, 1993.

Baedecker, M. J., Cozzarelli, I. M., Eganhouse, R. P., Siegel, D. I., and Bennett, P. C.: Crude oil in a shallow sand and gravel aquifer – III. Biogeochemical reactions and mass balance modeling in anoxic groundwater, Appl. Geochem., 8, 569–586, 1993.

Bahr, C. W.: Virgin oil field, Washington County, Utah, in: Guidbook to the geology of southwestern Utah: Transition between basin-range and Colorado plateau provinces, edited by: Heylmun, E. B., Intermountain Association of Petroleum Geologists, Salt Lake City, 169–171, 1963.

Bakker, R. J.: Package FLUIDS 1. Computer programs for analysis of fluid inclusion data and for modelling bulk fluid properties, Chem. Geol., 194, 3–23, 2003.

Ballentine, C. J., Burgess, R., and Marty, B.: Tracing Fluid Origin, Transport and Interaction in the Crust, in: Reviews in Mineralogy & Geochemistry – Noble Gases in Geochemistry and Cosmochemistry, edited by: Porcelli, D., Ballentine, C. J., and Wieler, R., Mineralogical Society of America, Washington D.C., 539–614, 2002.

Beck, W. C., Grossman, E. L., and Morse, J. W.: Experimental studies of oxygen isotope fractionation in the carbonic acid system at 15, 25, and 40 °C, Geochim. Cosmochim. Ac., 69, 3493–3503, 2005.

Benedicto, A., Plagnes, A., Vergely, P., Flotte, N., and Schultz, R. A.: Fault and fluid interaction in a rifted margin: integrated study of calcite-sealed fault-related structures (southern Corinth margin), in: The Internal Structure of Fault Zones: Implications for Mechanical and Fluid-Flow Properties, edited by: Wibberley, C. A. J., Kurz, W., Imber, J., Holdsworth, R. E., and Collettini, C., Geological Society of London, 257–275, 2008.

Bergman, S., Huntington, K. W., and Crider, J. G.: Tracing paleofluid sources using clumped isotope thermometry of diagenetic cements along the Moab Fault, Utah, Am. J. Sci., 313, 490–515, 2013.

Best, M. and Brimhall, W.: Late Cenozoic alkalic basaltic magmas in the western Colorado Plateaus and the Basin and Range transition zone, USA, and their bearing on mantle dynamics, Geol. Soc. Am. Bull., 85, 1677–1690, 1974.

Biek, R.: Geologic Map of the Hurricane Quadrangle Washington County, Utah: Utah Geological Survey Map, map no. 187, 2003.

Biek, R., Rowley, P., Hayden, J., Hacker, D., Willis, G., Hintze, L., Anderson, R., and Brown, K.: Geologic map of the St. George and east part of the Clover Mountains 30' × 60' quadrangles, Washington and Iron counties, Utah, Utah Geological Society, 2010.

Billingsley, G. and Workman, J.: Geological map of the Littlefield 30' × 60' quadrangle, Mohave County, northwestern Arizona, U.S.G.S, Reston, VA, 2000.

Billingsley, G. and Wellmeyer, J.: Geologic map of the Mount Trumbull 30' × 60' quadrangle, Mohave and Coconino Counties, northwestern Arizona, U.S.G.S., Reston, VA, 2003.

Blakey, R.: Oil impregnated carbonate rocks of the Timpoweap Member Moenkopi Formation, Hurricane Cliffs area, Utah and Arizona, Utah Geology, 6, 45–54, 1979.

Bodnar, R., Lecumberri-Sanchez, P., Moncada, D., and Steele-MacInnis, M.: 13.5 – Fluid inclusions in hydrothermal ore deposits, in: Treatise on Gechemistry, Second Edition, Elsevier, Oxford, 2014.

Bodnar, R. J.: Revised equation and table for determining the freezing point depression of H_2O-NaCl solutions, Geochim. Cosmochim. Ac., 57, 683–684, 1993.

Boles, J. R., Eichhubl, P., Garven, G., and Chen, J.: Evolution of a hydrocarbon migration pathway along basin-bounding faults: Evidence from fault cement, AAPG Bull., 88, 947–970, 2004.

Caine, J. S. and Minor, S. A.: Structural and geochemical characteristics of faulted sediments and inferences on the role of water in deformation, Rio Grande Rift, New Mexico, Geol. Soc. Am. Bull., 121, 1325–1340, 2009.

Caine, J. S., Evans, J. P., and Forster, C. B.: Fault zone architecture and permeability structure, Geology, 24, 1025–1028, 1996.

Caine, J. S., Bruhn, R. L., and Forster, C. B.: Internal structure, fault rocks, and inferences regarding deformation, fluid flow, and mineralization in the seismogenic Stillwater normal fault, Dixie Valley, Nevada, J. Struct. Geol., 32, 1576–1589, 2010.

Cao, J., Jin, Z., Hu, W., Zhang, Y., Yao, S., Wang, X., Zhang, Y., and Tang, Y.: Improved understanding of petroleum migration history in the Hongche fault zone, northwestern Junggar Basin (northwest China): Constrained by vein-calcite fluid inclusions and trace elements, Mar. Petrol. Geol., 27, 61–68, 2010.

Chan, M. A., Parry, W., and Bowman, J.: Diagenetic hematite and manganese oxides and fault-related fluid flow in Jurassic sandstones, southeastern Utah, AAPG Bull., 84, 1281–1310, 2000.

Chan, M. A., Parry, W. T., Petersen, E. U., and Hall, C. M.: $^{40}Ar/^{39}Ar$ age and chemistry of manganese mineralization in the Moab and Lisbon fault systems, southeastern Utah, Geology, 29, 331–334, 2001.

Chester, F. M., Evans, J. P., and Biegel, R. L.: Internal structure and weakening mechanisms of the San Andreas fault, J. Geophys. Res.-Sol. Ea., 98, 771–786, 1993.

Clayton, R. N., Friedman, I., Graf, D. L., Mayeda, T. K., Meents, W. F., and Shimp, N. F.: The origin of saline formation waters, I: Isotopic composition, J. Geophys. Res., 71, 3869–3882, 1966.

Crossey, L. J., Fischer, T. P., Patchett, P. J., Karlstrom, K. E., Hilton, D. R., Huntoon, P., Newell, D., and Reynolds, A.: Dissected hydrologic system at the Grand Canyon: Interaction between deeply derived fluids and plateau aquifer waters in modern springs and travertine, Geology, 34, 25–28, 2006.

Crossey, L. J., Karlstrom, K. E., Springer, A., Newell, D. L., Hilton, D. R., and Fischer, T. P.: Degassing of mantle-derived CO_2 and He from springs in the southern Colorado Plateau region – flux rates, neotectonic connections, and implications for groundwater systems, GSA Bulletin, 21, 1034–1053, 2009.

Crow, R., Karlstrom, K., Asmerom, Y., Schmandt, B., Polyak, V., and DuFrane, S. A.: Shrinking of the Colorado Plateau via lithospheric mantle erosion: Evidence from Nd and Sr isotopes and geochronology of Neogene basalts, Geology, 39, 27–30, 2011.

Deines, P., Langmuir, D., and Harmon, R. S.: Stable carbon isotope ratios and the existence of a gas phase in the evolution of carbonate ground waters, Geochim. Cosmochim. Ac., 38, 1147–1164, 1974.

Dietrich, D., McKenzie, J. A., and Song, H.: Origin of calcite in syntectonic veins as determined from carbon-isotope ratios, Geology, 11, 547–551, https://doi.org/10.1130/0091-7613(1983)11<547:OOCISV>2.0.CO;2, 1983.

Dutson, S.: Effects of Hurricane Fault Architecture on Groundwater Flow in the Timpoweap Canyon of Southwestern, Utah, MS thesis, Provo, Brigham Young University, 2005.

Edwards, R. L., Chen, J. H., and Wasserburg, G.: ^{238}U-^{234}U-^{230}Th-^{232}Th systematics and the precise measurement of time over the past 500,000 years, Earth Planet. Sc. Lett., 81, 175–192, 1987.

Eichhubl, P., Davatzes, N. C., and Becker, S. P.: Structural and diagenetic control of fluid migration and cementation along the Moab fault, Utah, AAPG Bull., 93, 653–681, 2009.

Evans, J. P., Forster, C. B., and Goddard, J. V.: Permeability of fault-related rocks, and implications for hydraulic structure of fault zones, J. Struct. Geol., 19, 1393–1404, 1997.

Fenton, C. R., Webb, R. H., Pearthree, P. A., Cerline, T. E., and Poreda, R. J.: Displacement rates on the Toroweap and Hurricane faults: Implications for Quaternary downcutting in the Grand Canyon, Arizona, Geology, 29, 1035–1038, 2001.

Fisher, J. R.: The volumetric properties of H_2O, J. Res. US Geol. Surv., 4, 189–193, 1976.

Forster, C. B. and Smith, L.: The influence of groundwater flow on thermal regimes in mountainous terrain: A model study, J. Geophys. Res., 94, 9439–9451, 1989.

Foxford, K., Walsh, J., Watterson, J., Garden, I. R., Guscott, S., and Burley, S.: Structure and content of the Moab Fault Zone, Utah, USA, and its implications for fault seal prediction, Geol. Soc. Lond. Spec. Publ., 147, 87–103, 1998.

Frery, E., Gratier, J.-P., Ellouz-Zimmerman, N., Loiselet, C., Braun, J., Deschamps, P., Blamart, D., Hamelin, B., and Sennen, R.: Evolution of fault permeability during episodic fluid circulation: Evidence for the effects fo fluid-rock interactions from travertine studies (Utah-USA), Tectonophysics, 651–652, 121–137, 2015.

Ghisetti, F., Kirschner, D., Vezzani, L., and Agosta, F.: Stable isotope evidence for contrasting paleofluid circulation in thrust faults and normal faults of the central Apennines, Italy, J. Geophys. Res.-Sol. Ea., 106, 8811–8825, 2001.

Gilfillan, S. M. V., Sherwood Lollar, B., Holland, G., Blagburn, D., Stevens, S., Schoell, M., Cassidy, M., Ding, Z., Zhou, Z., Lacrampe-Couloume, G., and Ballentine, C. J.: Solubility trapping in formation water as dominant CO_2 sink in natural gas fields, Nature, 458, 614–617, 2009.

Goldstein, R. H.: Fluid inclusions in sedimentary and diagenetic systems, Lithos, 55, 159–193, 2001.

Goldstein, R. H. and Reynolds, T. J.: Systematics of fluid inclusions in diagenetic minerals/SEPM Short Course 31, Society for Sedimentary Geology, Tulsa, OK, 199 pp., 1994.

Heller, P., Bowdler, S., Chambers, H., Coogan, J., Hagen, E., Shuster, M., Winslow, N., and Lawton, T.: Time of initial thrusting in the Sevier orogenic belt, Idaho-Wyoming and Utah, Geology, 14, 388–391, 1986.

Hendy, C. H.: The isotopic geochemistry of speleothems – I. The calculation of the effects of different modes of formation on the isotopic composition of speleothems and their applicability as palaeoclimatic indicators, Geochim. Cosmochim. Ac., 35, 801–824, 1971.

Heynekamp, M. R., Goodwin, L. B., Mozley, P. S., and Haneberg, W. C.: Controls on fault-zone architecture in poorly lithified sediments, Rio Grande Rift, New Mexico: Implications for fault-zone permeability and fluid flow, Washington DC American Geophysical Union Geophysical Monograph Series, 113, 27–49, 1999.

Hodson, K. R., Crider, J. G., and Huntington, K. W.: Temperature and composition of carbonate cements record early structural control on cementation in a nascent deformation band fault zone: Moab Fault, Utah, USA, Tectonophysics, 690, 240–252, 2016.

Hoefs, J.: Stable Isotope Geochemistry, 3rd Edn., Springer-Verlag, New York, 241 pp., 1987.

Humphreys, E., Hessler, E., Dueker, K., Farmer, G. L., Erslev, E., and Atwater, T.: How Laramide-age hydration of North American lithosphere by the Farallon Slab controlled subsequent activity in the Western United States, Int. Geol. Rev., 45, 575–595, 2003.

Kampman, N., Burnside, N. M., Shipton, Z. K., Chapman, H. J., Nicholl, J. A., Ellam, R. M., and Bickle, M. J.: Pulses of carbon dioxide emissions from intracrustal faults following climatic warming, Nat. Geosci., 5, 352–358, 2012.

Kim, S.-T., Coplen, T. B., and Horita, J.: Normalization of stable isotope data for carbonate minerals: Implementation of IUPAC guidelines, Geochim. Cosmochim. Ac., 158, 276–289, 2015.

Knipe, R.: Faulting processes and fault seal, in: Structural and tectonic modelling and its application to petroleum geology, Proceedings of Norwegian Petroleum Society Workshop, 18–20 October 1989, Stavanger, Norway, edited by: Larsen, R. M., Brekke, H., Larsen, B. T., and Talleraas, E., Elsevier, Amsterdam, 325–342, 1992.

Koger, J. M.: Spatio-Temporal History of Fluid-Rock Interaction in the Hurricane Fault Zone, MS, Utah State University, 158 pp., 2017.

Krüger, Y., Stoller, P., Rička, J., and Frenz, M.: Femtosecond lasers in fluid-inclusion analysis: overcoming metastable phase states, Eur. J. Mineral., 19, 693–706, 2007.

Laubach, S. E., Eichhubl, P., Hilgers, C., and Lander, R.: Structural diagenesis, J. Struct. Geol., 32, 1866–1872, 2010.

Laubach, S. E., Lander, R., Criscenti, L. J., Anovitz, L. M., Urai, J., Pollyea, R., Hooker, J. N., Narr, W., Evans, M. A., and Kerisit, S. N.: The role of chemistry in fracture pattern development and

opportunities to advance interpretations of geological materials, Rev. Geophys., 57, 1065–1111, 2019.

Livaccari, R. F.: Role of crustal thickening and extensional collapse in the tectonic evolution of the Sevier-Laramide orogeny, western United States, Geology, 19, 1104–1107, 1991.

Lund, W., Hozik, M., and Hatfield, S.: Paleoseismic investigation and long-term slip history of the Hurricane Fault in southwestern Utah, Paleoseismology of Utah, Vol. 14, Utah Geological Survery, Salt Lake City, UT, 81 pp., 2007.

Marty, B. and Jambon, A.: $C/^3He$ in volatile fluxes from the solid Earth: Implications for carbon geodynamics, Earth Planet. Sc. Lett., 70, 196–206, 1987.

McCrea, J. M.: On the isotope chemistry of carbonates and a paleotemperature scale, J. Chem. Phys., 18, 849–857, 1950.

Mozafari, M., Swennen, R., Balsamo, F., Clemenzi, L., Storti, F., El Desouky, H., Vanhaecke, F., Tueckmantel, C., Solum, J., and Taberner, C.: Paleofluid Evolution In Fault-Damage Zones: Evidence From Fault–Fold Interaction Events In the Jabal Qusaybah Anticline (Adam Foothills, North Oman), J. Sediment. Res., 85, 1525–1551, 2015.

Mozley, P. S. and Goodwin, L. B.: Patterns of cementation along a Cenozoic normal fault: A record of paleoflow orientations, Geology, 23, 539–542, 1995.

Nelson, S. T. and Tingey, D. G.: Time-transgressive and extension-related basaltic volcanism in southwest Utah and vicinity, Geol. Soc. Am. Bull., 109, 1249–1265, 1997.

Nelson, S. T., Mayo, A. L., Gilfillan, S., Dutson, S. J., Harris, R. A., Shipton, Z. K., and Tingey, D. G.: Enhanced fracture permeability and accompanying fluid flow in the footwall of a normal fault: The Hurricane fault at Pah Tempe hot springs, Washington County, Utah, Geol. Soc. Am. Bull., 109, 1249–1265, 2009.

Newell, D. L., Jessup, M. J., Cottle, J. M., Hilton, D., Sharp, Z., and Fischer, T.: Aqueous and isotope geochemistry of mineral springs along the southern margin of the Tibetan plateau: Implications for fluid sources and regional degassing of CO_2, Geochem. Geophy. Geosy., 9, Q08014, https://doi.org/10.1029/2008GC002021, 2008.

Newell, D. and Koger, J.: Calcite vein C and O stable isotope values, fluid inclusion microthermometry, and U-Th dates from the Hurricane Fault zone, Utah and Arizona, USA., Version 1.0. Interdisciplinary Earth Data Alliance (IEDA), https://doi.org/10.26022/IEDA/111542, 2020.

Newell, D. L., Jessup, M. J., Hilton, D. R., Shaw, C. A., and Hughes, C. A.: Mantle-derived helium in hot springs of the Cordillera Blanca, Peru: Implications for mantle-to-crust fluid transfer in a flat-slab subduction setting, Chem. Geol., 417, 200–209, 2015.

Nuriel, P., Rosenbaum, G., Uysal, T. I., Zhoa, J. X., Golding, S. D., Weinberger, R., Karabacak, V., and Avni, Y.: Formation of fault-related calcite precipitates and their implications for dating fault activity in the East Anatolian and Dead Sea fault zones, Geol. Soc. Lond. Spec. Publ., 359, 229–248, 2011.

Nuriel, P., Weinberger, R., Rosenbaum, G., Golding, S. D., Zhao, J., Tonguc Uysal, I., Bar-Matthews, M., and Gross, M. R.: Timing and mechanism of late-Pleistocene calcite vein formation across the Dead Sea Fault Zone, northern Israel, J. Struct. Geol., 36, 43–54, 2012.

O'Neil, J. R., Adami, L. H., and Epstein, S.: Revised value for the ^{18}O fractionation between CO_2 and H_2O at 25 °C, J. Res. US Geol. Surv., 3, 623–624, 1975.

O'Neil, R. R., Clayton, R. N., and Mayeda, T. K.: Oxygen isotope fractionation in divalent metal carbonates, J. Chem. Phys., 51, 5547–5558, 1969.

Pearthree, P. A., Menges, C. M., and Mayer, L.: Distribution, recurrence, and possible tectonic implications of late Quaternary faulting in Arizona, Tucson, AZ, Arizona Geological Survey OFR-83-20, 36 pp., 1983.

Quigley, M. C., Karlstrom, K., and Kelley, S.: Influence of Proterozoic and Laramide structures on the Miocene extensional strain field, SE Nevada, Geological Society of America Abstracts with Programs, Geological Society of America, Boulder, CO, 2002.

Quirk, B. J., Mackey, G. N., Fernandez, D. P., Armstrong, A., and Moore, J. R.: Speleothem and glacier records of Late Pleistocene-Early Holocene climate change in the Western North American Interior, J. Quaternary Sci., 35, 776–790, 2020.

Ramsay, J. G.: The crack-seal mechanism of rock deformation, Nature, 284, 135–139, 1980.

Rowley, P., Williams, V., Vice, G., Maxwell, D., Hacker, D., Snee, L., and Mackin, J.: Interim geologic map of the Cedar City 30' x 60' quadrangle, Iron and Washington Counties, Utah, Utah Geological Society, 2008.

Salomon, E., Rotevatn, A., Kristensen, T. B., Grundvåg, S.-A., Henstra, G. A., Meckler, A. N., Gerdes, A., and Albert, R.: Fault-controlled fluid circulation and diagenesis along basin bounding fault systems in rifts – insights from the East Greenland rift system, Solid Earth Discuss., https://doi.org/10.5194/se-2020-72, in review, 2020.

Sharp, Z. D.: Principles of Stable Isotope Geochemistry, Pearson/Prentice Hall, Upper Saddle River, N.J., 344 pp., 2007.

Sherwood Lollar, B., Ballentine, C. J., and O'Nions, R. K.: The fate of mantle-derived carbon in a continental sedimentary basin: Integration of C/He relationships and stable isotope signatures, Geochim. Cosmochim. Ac., 61, 2295–2307, 1997.

Shipton, Z. K., Evans, J. P., Kirschner, D., Kolesar, P. T., Williams, A. P., and Heath, J.: Analysis of CO_2 leakage through 'low-permeability'faults from natural reservoirs in the Colorado Plateau, east-central Utah, Geol. Soc. Lond. Spec. Publ., 233, 43–58, 2004.

Sibson, R. H.: Crustal stress, faulting and fluid flow, Geol. Soc. Lond. Spec. Publ., 78, 69–84, 1994.

Sibson, R. H.: Structural permeability of fluid-driven fault-fracture meshes, J. Struct. Geol., 18, 1031–1042, 1996.

Sibson, R. H.: Fluid involvement in normal faulting, J.Geodyn., 29, 469–499, 2000.

Smeraglia, L., Bernasconi, S. M., Berra, F., Billi, A., Boschi, C., Caracausi, A., Carminati, E., Castorina, F., Doglioni, C., and Italiano, F.: Crustal-scale fluid circulation and co-seismic shallow comb-veining along the longest normal fault of the central Apennines, Italy, Earth Planet. Sc. Lett., 498, 152–168, 2018.

Smith, R. B., Nagy, W. C., Julander, K., Viveiros, J. J., Barker, C. A., and Gants, D. G.: Geophysical and tectonic framework of the eastern Basin and Range-Colorado Plateau-Rocky Mountain transition, in: Geophysical Framework of the Continental United States, Geol. Soc. Am. Mem Boulder, CO, 205–233, 1989.

Sommer, S. N. and Budding, K. E.: Low-temperature thermal waters in the Santa Clara and Virgin River valleys, Washington County, Utah, in: Cenozoic Geology and Geothermal Systems of Southwestern Utah, edited by: Blackett, R. E. and Moore, J., Utah Geological Association, Salt Lake City, 81–95, 1994.

Stenner, H. D. and Pearthree, P. A.: Paleoseismology of the southern Anderson Junction section of the Hurricane Fault, northwestern Arizona and southwestern Utah, Arizona Geological Survery, Tucson, Arizona Geological Survey, Tucson, AZ, Open-File Report 99-8, 1999.

Stewart, M. E. and Taylor, W. J.: Structural analysis and fault segment boundary identification along the Hurricane fault in southwestern Utah, J. Struct. Geol., 18, 1017–1029, 1996.

Swanson, E. M., Wernicke, B. P., Eiler, J. M., and Losh, S.: Temperatures and fluids on faults based on carbonate clumped–isotope thermometry, Am. J. Sci., 312, 1–21, 2012.

Tuccillo, M. E., Cozzarelli, I. M., and Herman, J. S.: Iron reduction in the sediments of a hydrocarbon-contaminated aquifer, Appl. Geochem., 14, 655–667, 1999.

USGS: ANSS Comprehensive Earthquake Catalog, available at: https://earthquake.usgs.gov/earthquakes/search/, last access: 20 April 2020.

USGS EROS Archive: Digital Elevation – Shuttle Radar Topography Mission (SRTM) 1 Arc-second Global: https://www.usgs.gov/centers/eros, last access: September 2019.

Walk, C. J., Karlstrom, K. E., Crow, R. S., and Heizler, M. T.: Birth and evolution of the Virgin River fluvial system: $\sim$ 1 km of post–5 Ma uplift of the western Colorado Plateau, Geosphere, 15, 759–782, 2019.

Watkins, H., Bond, C. E., Healy, D., and Butler, R. W.: Appraisal of fracture sampling methods and a new workflow to characterise heterogeneous fracture networks at outcrop, J. Struct. Geol., 72, 67–82, 2015.

Williams, R. T., Goodwin, L. B., Mozley, P. S., Beard, B. L., and Johnson, C. M.: Tectonic controls on fault zone flow pathways in the Rio Grande rift, New Mexico, USA, Geology, 43, 723–726, 2015.

Williams, R. T., Goodwin, L. B., and Mozley, P. S.: Diagenetic controls on the evolution of fault-zone architecture and permeability structure: Implications for episoldicity of fault-zone fluid transport in extensional basins, Geol. Soc. Am. Bull., 129, 464–478, 2017a.

Williams, R. T., Goodwin, L. B., Sharp, W. D., and Mozley, P. S.: Reading a 400,000-year record of earthquake frequency for an intraplate fault, P. Natl. Acad. Sci. USA, 114, 4893–4898, 2017b.

Williams, R. T., Beard, B. L., Goodwin, L. B., Sharp, W. D., Johnson, C. M., and Mozley, P. S.: Radiogenic isotopes record a "drop in a bucket" – A fingerprint of multi-kilometer-scale fluid pathways inferred to drive fault-valve behavior, J. Struct. Geol., 125, 262–269, 2019.

Yardley, B., Banks, D., Barnicoat, A., and Porter, T.: The chemistry of crustal brines: tracking their origins, in: Hydrothermal iron oxide copper-gold and related deposits: A global perspective, edited by: Porter, T., Porter Geological Publishing, Adelaide, 61–70, 2000.

Yonkee, W. A. and Weil, A. B.: Tectonic evolution of the Sevier and Laramide belts within the North American Cordillera orogenic system, Earth-Sci. Rev., 150, 531–593, 2015.

Zandt, G., Myers, S. C., and Wallace, T. C.: Crust and mantle structure across the Basin and Range-Colorado Plateau boundary at 37° N latitude and implications for Cenozoic extensional mechanism, J. Geophys. Res.-Sol. Ea., 100, 10529–10548, 1995.